Chapter 3

Two-Phase Physical Modelling

3.1 Interfacial Source Terms

Along with the basic conservation laws, the most important work in deriving the nonequilibrium, two-phase flow equations is the modeling of interfacial effects. Three such effects (interfacial momentum, heat, and mass transfer) are possible and yield complicated source terms and coupling between the equations. Several simplifying assumptions need to be made with regard to interfacial effects to keep the computational effort tractable.

One of these which applies to all the interfacial terms is that either bubbly or droplet flow prevails throughout the ejector. Based on flow regime maps and experimental observation this has been shown to be true for most of the domain of interest. Bubbly flow is present in the bubbly flow tube leading to the motive nozzle. Within the nozzle, the bubbles expand as the pressure decreases and soon enough vapor is formed so that by the nozzle outlet a droplet flow is visible. Droplet flow then continues through the mixing section and diffuser. In the motive nozzle it is assumed for simplicity that a sharp break exists between the bubbly and droplet flow regimes, although in reality some transitional regime is present. A preliminary criterion for when the break occurs is based on a volume fraction of 50%. This number may be adjusted in light of new information on flow regimes or the results of the computation.

3.1.1 Momentum Transfer

The simplest interfacial effect is momentum transfer which results from unequal velocities between the two phases. Drag between a fast moving droplet and slow moving vapor, for instance, tends to slow down the droplet and speed up the surrounding vapor as well as cause some frictional heating of both phases due to viscous dissipation. A simple model is proposed in which the interfacial drag force depends on a drag coefficient which is assumed to be the same as for a solid sphere. The interfacial drag force is thus given by:

$$F_x = \frac{3\rho_{cont}\alpha_{disc}C_D}{4d_{disc}}\left|\vec{V}_{other} - \vec{V}\right|(u_{other} - u) \tag{3.1}$$

The velocity difference between the phases is broken up using the absolute value sign as shown to ensure that the drag force is positive on the slower moving phase, and negative on the faster moving phase. A large number of formulae are available for sphere drag coefficient (C_D) as a function of Reynolds number. It is assumed that the droplets or bubbles are small enough to be nearly spherical.

The formula for C_D used here is from the work of Ishii and Mishima [24]:

$$C_D = \frac{24(1 + .1Re_{int}^{.75})}{Re_{int}} \tag{3.2}$$

The interfacial Reynold's number is simply:

$$Re_{int} = \frac{2r_d\rho_c V_r}{\mu_m} \tag{3.3}$$

where V_r is the relative velocity between the phases:

$$V_r = \sqrt{(u_l - u_v)^2 + (v_l - v_v)^2} \tag{3.4}$$

The mixture viscosity, μ_m, used above is based on simple formulae provided by Ishii and Mishima [24] which are functions of the flow regime and volume fraction. It is a modification of the continuous phase viscosity to correct for the presence of the discontinuous phase. Indeed, the drag coefficient used here is essentially the same as for individual sphere drag with some modifications to allow for the effects of interaction among many such spheres.

Another interfacial term in the momentum equation relates the momentum transferred between phases due to evaporation or condensation. The formula for this effect is:

$$M_x = MAX[\Gamma, 0]u_{other} - MAX[-\Gamma, 0]u \tag{3.5}$$

Here it is noted that positive Γ, which means mass is being added to phase *i*, corresponds to a positive addition of momentum. Whatever momentum gained by one phase through evaporation or condensation is lost equally by the other.

3.1.2 Energy and Mass Transfer

Interfacial energy transfer is somewhat more complex than momentum. Interfacial heat transfer effects must be modelled which in turn affect the evaporation or condensation rate. Terms which represent viscous dissipation also arise.

The thermal energy transferred (sensible heat) due to evaporation or condensation can be expressed as:

$$E_{mt} = c_p T \Gamma \tag{3.6}$$

The next two effects, interfacial heat and mass transfer, are strongly coupled. Interfacial heat transfer occurs when the liquid and vapor phases are at unequal temperatures. Assuming a droplet flow for purposes of discussion, Figure 3.1 gives an example heat balance of a superheated liquid droplet in a superheated vapor. The interface itself is at the saturation temperature so conduction between it and the discontinuous phase and convection between it and the continuous phase occurs. Since the interface cannot store energy the sum of all heat fluxes to it must equal zero. Thus any imbalance between conduction and convection is made up for by evaporation or condensation, which is the interfacial mass transfer. The model used here is based on the work of Solbrig et al. [38].

The heat transfer rate (either conduction or convection) between the interfacial surface and the bulk phase can be generally represented as:

$$E_{ht} = h(T_S - T)\left(\frac{6\alpha_{disc}}{d_{disc}}\right) \tag{3.7}$$

The last term in parenthesis in this equation represents the surface area of each particle (droplet or bubble) times the number of particles per control volume, as required to ensure consistent units. Note that two such equations are needed, one for the liquid and the other for the vapor.

The Solbrig et al. [38] model includes methods to find the heat transfer coefficient, *h*, for the various combinations of conduction and convection in both bubbly and droplet flows. The interfacial mass transfer can now be found by relating the boiling heat transfer to the latent heat of evaporation of the fluid:

$$\Gamma = \pm\frac{E_{ht,L} + E_{ht,V}}{h_{fg}} \tag{3.8}$$

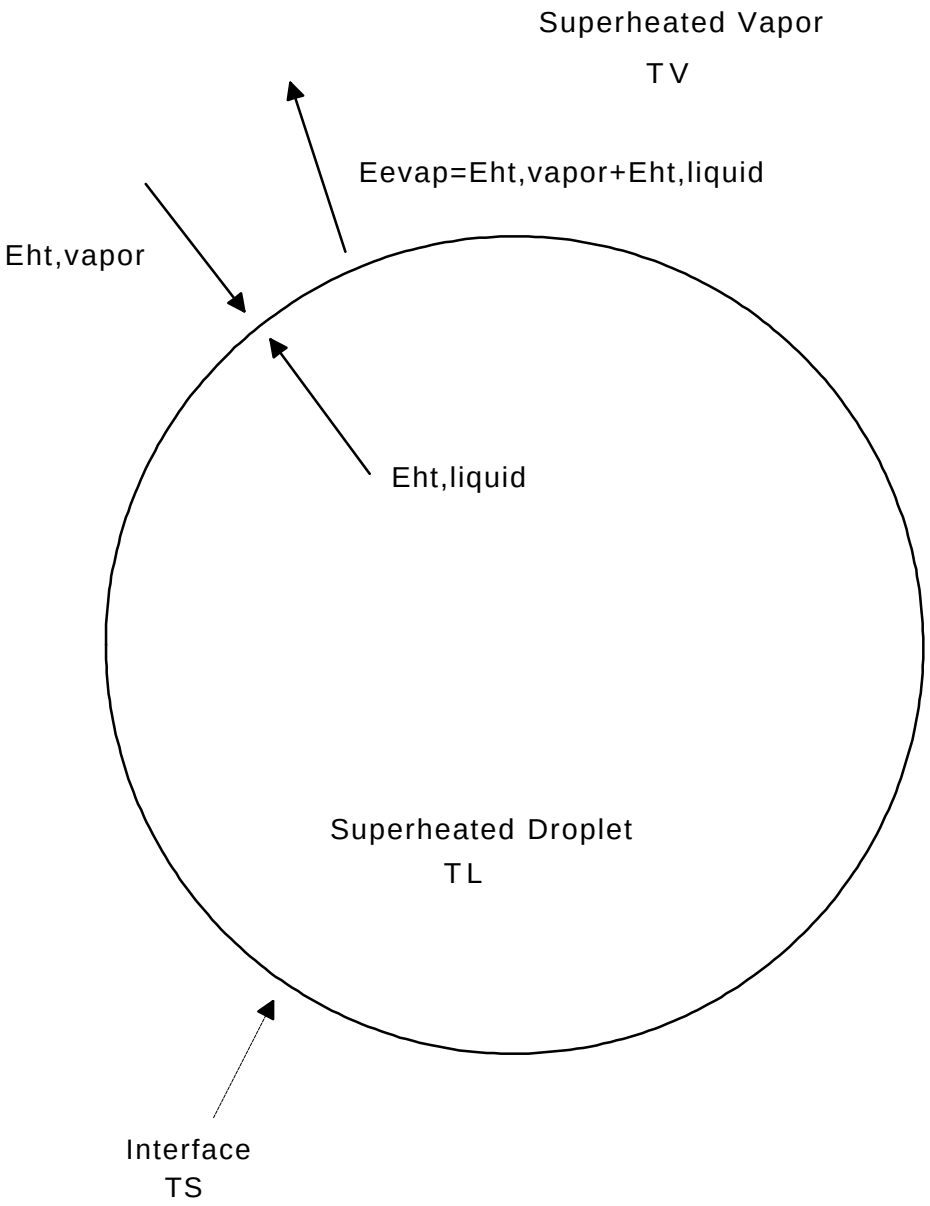

Figure 3.1 - Energy Balance on Droplet

The sign and magnitude of the heat transfer terms for liquid and vapor are important and determine whether evaporation or condensation occur. In general if the net heat transfer to the interface is positive (ie *negative* $E_{ht,L}$+$E_{ht,V}$), evaporation takes place and if the net heat transfer to the interface is negative (ie *positive* $E_{ht,L}$+$E_{ht,V}$), condensation takes place. This means that the positive sign in Eqn. 3.8 must be for the liquid phase and the negative sign must be for the vapor phase.

Another source term in the energy equation relates the kinetic energy transferred due to mass transfer:

$$E_{ke} = MAX[\Gamma, 0]\left(\frac{1}{2}u_{other}^2 + \frac{1}{2}u^2 - uu_{other}\right) \tag{3.9}$$

This term is actually viscous dissipation, a fact which can be verified by noting the manner in which it is derived (Appendix B). Essentially, this is a term which is left over from the subtraction of the mechanical energy equation from the thermal energy equation. Since the phases generally move at unequal velocities, any mass transferred between them must equilibrate to the new phase's velocity, an effect which results in dissipation. The dissipation is assumed to always be in the phase to which mass is added.

The last source term in the energy equation is the viscous dissipation produced by work of the interfacial drag force. This term is given by:

$$W_{int} = \frac{1}{2}(u_{other} - u)F_x \tag{3.10}$$

Again, this term is always positive because when the velocity difference is positive the interfacial drag force is also positive. Conversely, when the velocity difference is negative the drag force is also negative. The factor of 1/2 assumes that each phase receives an equal share of the total dissipation. Note that both these interfacial effects are neglected in

the thermal energy expression as shown in Sec. 2.2.3. This move is in keeping with neglecting all viscous dissipation, whether it is single-phase or two-phase. More importantly, these terms can be shown to be negligible by a simple numerical example. They are included mainly for completeness.

Also neglected are work terms having to do with pressure differences across curved boundaries with surface tension, such as the surface of a droplet.

3.2 Flow Regime Determination

The flow regime plays an important role in determining the form of the interfacial source terms. Using a combination of theory and empirical results, researchers have determined forms for such parameters as interfacial heat transfer and drag coefficient for several different flow regimes (see, for instance, Solbrig, et al. [38]). In the ejector, the flow regime changes from bubbly to droplet flow within the motive nozzle. It then remains as a droplet flow throughout the mixing section and diffuser. The changeover from bubbly to droplet flow may involve an intermediate flow regime or it may occur in a sudden shock-like fashion. It will be assumed here that that the transition takes place suddenly, both for simplicity and because experimental evidence exists for a shock-like flow regime transition.

By what criterion does the break between bubbly and droplet flow occur? Usually, workers use flow regime maps which give the flow regime as a function of important two-phase flow variables such as superficial gas and liquid velocity. For this work, the flow regime map of Baker [39] would be suitable because it distinguishes clearly between a dispersed bubbly and dispersed droplet flow. However, this map, as with most others, has the disadvantage of not having been tested with refrigerants. Indeed, most testing is

done with only air and water. A map by Weisman [40] was found which used refrigerant 113, but unfortunately it did not distinguish the bubbly from the droplet regime.

Given the uncertainty of using published flow regime maps for this problem, a simpler criterion is advanced for determining the break between bubbly and droplet flow. It is known from both observation and flow regime maps that the flow entering and exiting the motive nozzle is in the dispersed bubbly and droplet regime, respectively. Furthermore, a typical value of the void fraction in the bubbly flow tube is 0.9, while at the motive nozzle exit it is about 0.1. This suggests an average value of 0.5 as the break point. This number may require modification in light of computational results or new evidence from flow regime maps.

3.3 Droplet/Bubble Size

Another important parameter in establishing accurate interfacial models is the determination of bubble and droplet size. This parameter appears in the calculation of interfacial drag and heat transfer rate. Again, several essentially empirical reports exist on the topic. None, however deals with refrigerants specifically.

Most work in this area is based on the theory of Hinze [41] and Kolmogoroff [42], which states that the maximum bubble or drop size is governed by a critical Weber number, which is the ratio of forces tending to break up the particle (turbulent fluctuations) to the forces which keep it together (surface tension):

$$We'_{crit} = \frac{\rho v^2}{\sigma / d_{max}} \left(\frac{\rho_d}{\rho_c} \right)^{1/3} \tag{3.11}$$

where v here is the average fluctuating velocity of the turbulent dispersion. Hesketh et al. [43] modify this formula by including additional effects and fluid properties to make it more generally applicable. The result is a formula which can be used to directly calculate the maximum particle size (bubble or droplet) as follows:

$$d_{max} = \frac{1.38(We_{crit}\sigma)^{0.6} D^{0.5}}{\rho_c^{0.3}\rho_d^{0.2}\mu_c^{0.1}v_c^{1.1}} \tag{3.12}$$

The critical Weber number (We_{crit}) here is taken as unity. This equation has the advantage of having been tested with several different mixtures (none refrigerants, however) and has some generality in terms of physical properties.

Although this formula is regarded as the most up-to-date, it yields much different results from other formulas for droplet sizing. Indeed, all the formulas exhibit a wide range of variation. Since no experimental measurements of droplet size have been taken for the EERC system, it is unclear which formula gives the most accurate results. Furthermore, all formulae are for equilibrium droplet sizes and it is not clear that, given the speed at which flow traverses the ejector, that equlibrium sizes are ever reached. Droplet diameter was, as a result, essentially assumed to be a variable in the model which, within reason, could be used to fit code results to experimental data.

3.4 Turbulence Model

Of major importance in this work is turbulence modelling. Throughout the ejector the flow is known from observation and calculation of the Reynold's number to be highly turbulent. Several well known methods are available to incorporate the effect of turbulence. The simplest method, the one chosen here, is Prandtl's mixing length model. Here, the Boussinesq assumption is inherent, in which all the effects of turbulence can be

incorporated into a single turbulent viscosity. The turbulent viscosity is simply added to the laminar viscosity for solution of the momentum equation. Hence, the basic equations do not change form and the solution method is the same as for the laminar case.

The mixing length model predicts the turbulent viscosity as follows:

$$\mu_t = \rho l_m^2 \frac{\partial u}{\partial r} \tag{3.13}$$

The mixing length l_m depends on the type of flow which is present and its location in the duct. For the motive and suction nozzle, the turbulence is driven by the wall. Thus, the turbulent wall layer grows in the axial direction until it fills the entire cross-section of the domain. For the mixing section, the wall layer is important as well as the shear layer in which the motive and suction flows mix. As shown in Fig. 3.2, both these layers grow into the undisturbed region of the flow until they meet. Both the wall dominated and jet shear dominated flows have distinct expressions for the mixing length.

According to turbulent flow theory the wall region can be subdivided into a wall sublayer, an overlap region, and an outer layer. For flow within the wall sublayer and logarithmic overlap region (inner layer), the mixing length is estimated by the textbook van Driest damping function as:

$$l_m = \kappa(r_t - r)\left[1 - \exp\left(-\frac{(r_t - r)(\rho\tau_w)^{1/2}}{\mu A}\right)\right] \quad \text{where} \quad \kappa = 0.6 \quad \text{and} \quad A = 26 \tag{3.14}$$

The values shown for κ and A have been found to give good results for both single and two-phase simulations of the code. For the outer layer of the wall region, the mixing length is constant:

$$l_m = 0.09\delta_{wall} \quad \text{where} \quad \delta_{wall} \text{ is the thickness of the wall layer} \tag{3.15}$$

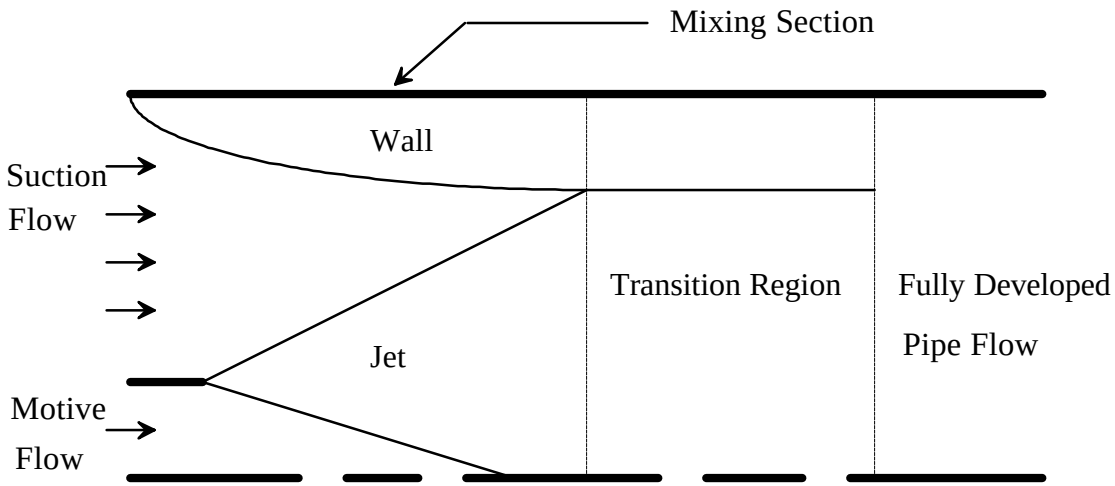

Figure 3.2 - Turbulent Boundary Layer Regions in Mixing Section

The transition between the inner and outer layer occurs when the mixing length predicted by Eqn. 3.15 first exceeds the value of the mixing layer predicted by Eqn. 3.14.

For the jet region, a constant mixing length proportional to layer thickness is also used:

$$l_m = \kappa_0 \delta_{jet} \quad \text{where} \quad \kappa_0 = .08 \tag{3.16}$$

In the regions that are still undisturbed by turbulent shear, a mixing length of zero is assigned.

The mixing lengths found by these standard formulas can then be used in Eqn. 3.13 to find the turbulent viscosity. The viscosity obtained is then simply added to the molecular viscosity of the fluid and inserted into the momentum equation for solution.

As shown in Fig. 3.2 the jet region expands with the mixing process into the two undisturbed regions. The wall region also grows into the undisturbed region, and eventually meets the jet. It is assumed that after this point the thickness of the wall region and jet region remain constant. Although it is known that the wall eventually dominates the flow far downstream (jet gradually dissipates), the ejector mixing section and diffuser is not long enough to where this effect is appreciable. Thus the assumption of constant thickness after the meeting point is justified.

The thicknesses of the turbulent boundary layers themselves are calculated iteratively using the velocity profiles. Changes in the profile indicate that turbulent shear is prevalent. Conversely, if the profile doesn't change, turbulent shear has not yet affected the region. For the wall profile, for instance, the code begins at the wall and moves away, calculating the slope of the velocity profile at each step. The slope is expected to change (compared to the last axial step) due to the influence of the wall. When the slope stops changing the procedure knows that the wall thickness has been found by how far it has traversed into

the duct. A similar approach is used for the jet thickness. Since the turbulent viscosity and the velocity profile affect each other so strongly, this procedure must be iterative.

For turbulent conductivity, present in the energy equation, a common engineering approximation is that the turbulent Prandtl number is equal to one:

$$Pr_t = \frac{c_p \mu_t}{k_t} = 1 \tag{3.17}$$

Thus, only the turbulent viscosity calculated earlier, and this simple formula are required to introduce the effect of turbulence into the thermal energy equation. As with viscosity, the turbulent conductivity is added to the molecular conductivity to produce a total effective conductivity.

3.4.1 Wall Function Approximation

Introduction of turbulence into a CFD calculation greatly increases the fineness of the grid required to resolve the velocity profile, especially in regions near the wall. Since the grid proposed here is of constant size throughout the crossection, this situation would lead to using several thousand grid points in the radial direction when only a fine grid near the wall was needed.

The usual procedure for handling this situation is to use grid refinement only near the wall, either by doing a coordinate transformation or by using unequal grid spacing. Although computationally effective, this alternative is somewhat costly in terms of the re-formulation and re-coding that would have to be done for this problem. Since the turbulence model was added to a laminar code which had already been written, the requirements on grid refinement near the wall were not clearly understood when the problem was originally set up.

A simpler alternative is to use wall functions to eliminate the need for a fine grid near the wall. In this manner no changes are made to the original grid, although some procedural changes are required in the computation. The wall function approximation uses a form of the universal law of the wall in which velocity can be expressed as a function of wall shear and fluid properties:

$$u(r) = \left(\frac{\tau_w}{\rho}\right)^{1/2} \frac{1}{\kappa} \ln\left[\frac{(\rho\tau_w)^{1/2}}{\mu}(r_t - r)\right] + B \quad \text{where} \quad B = 5.0,\ \kappa = 0.6 \tag{3.18}$$

This formula is valid in the log-law region of the flow, $30<(r_t\text{-}r)^+<200$, where:

$$(r_t - r)^+ = \frac{(r_t - r)(\rho\tau_w)^{1/2}}{\mu} \tag{3.19}$$

The velocity profile according to the law of the wall can thus be computed up to $(r_t\text{-}r)^+=200$. The velocity at this outer point then becomes the upper boundary condition for the momentum equation in which the rest of the velocity profile in the domain is computed. This procedure is straightforward except that the wall shear in Eqn. 3.18 is not known a priori. The wall shear force is one of the critical components of the global momentum balance which must be satisfied. Thus the procedure involves an iteration on wall shear stress as follows:

1. Guess the wall shear stress (τ_w). An educated guess in this direction can be made using the Blasius formula for pipe flow (White, p. 423 [44]) $\tau_w = 0.0396\rho^{3/4} u_{ave}^{7/4} \mu^{1/4} D^{-1/4}$ for the first axial step, and the upstream value for the remaining steps.
2. Use the wall function formula (Eqn. 3.18) to get the velocity profile for the near-wall region: $30<(r_t\text{-}r)^+<200$

3. Using the wall profile as a boundary condition, solve for the remaining points in the duct by solving the momentum and continuity equations.
4. Using the entire velocity profile now obtained, and the guessed wall shear, establish whether or not global conservation of momentum across the duct is satisfied. If it is, then the guess for wall shear in step 1 was correct. If it is not, then guess the wall shear again, return to step 2, and repeat the calculation.

This iterative process appears to work well for single phase versions of the code. For a typical computation it reduces the radial grid points required from 2000 to approximately 120. Thus a tremendous savings of computer time is achieved with a very small sacrifice in accuracy. See Fig. 3.3 for velocity profiles calculated by this example.

The procedure outlined above is used for the solution of the continuous phase velocity profile. For the discontinuous phase, the same procedure could be used computationally but it is inconvenient to do so. As the wall is approached the velocity of the discontinuous phase approaches the velocity of the continuous phase because both velocities and tending toward zero and because of interfacial drag. If the approximation is made that the profiles are exactly equal to each other, then the ratio of the wall shear stresses for each phase is equal to the ratio of viscosities. This enables the direct calculation of the second phase wall shear stress:

$$\tau_{w2} = \tau_{w1} \frac{\mu_2}{\mu_1} \tag{3.20}$$

The momentum equation for the second phase can now be solved using as a boundary condition the known wall shear stress. This simplification avoids having to repeat the iterative wall function procedure for the discontinuous phase.

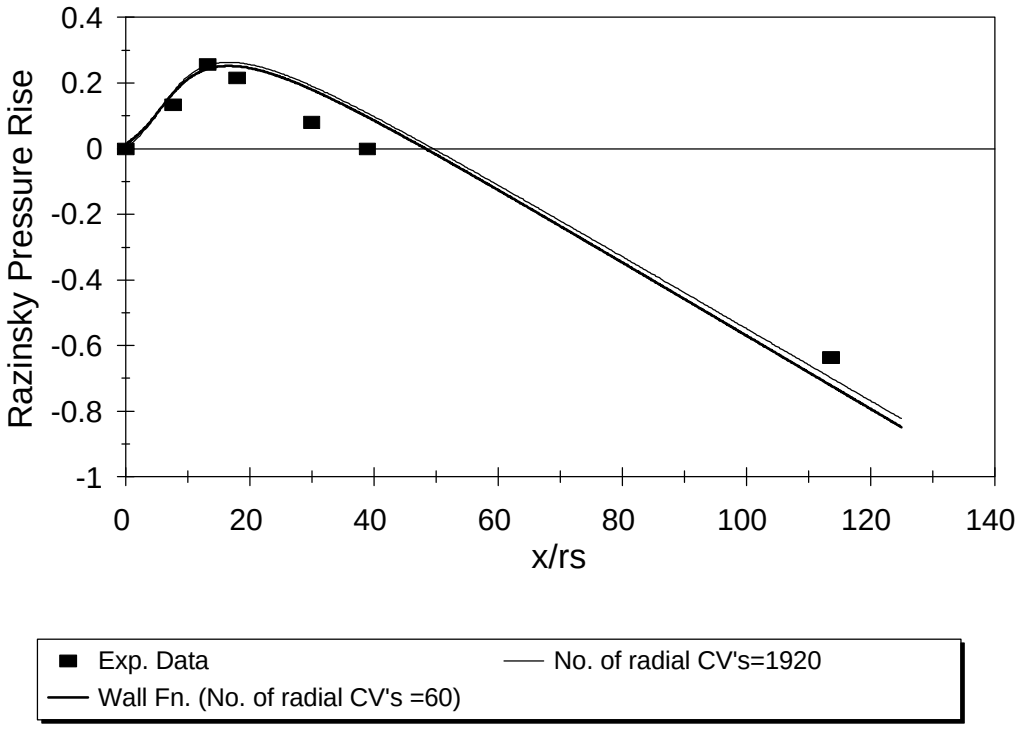

Figure 3.3 - Wall Function vs. Fine Grid and Exp. Data (Razinsky, et al. [45])

3.5 Refrigerant Thermo-Physical Properties

The thermodynamic properties of R134a are needed to solve this problem. A refrigerant properties database is available from NIST [46] which can be accessed through FORTRAN subroutine calls. However, these routines are computationally slow and given the number of times they would need to be accessed in a CFD code, their use would substantially retard execution of the code. They were used, however, in determining properties for cases in which constant properties could be assumed, as for instance, in the ejector mixing section. These are the cases that are presented in Chapter 5.

However, for future work, a set of approximations would need to be made which are simpler and faster to compute. Kornhauser [47] has begun work on such a set of thermodynamically consistent approximations. It remains for future work to incorporate these approximations into the code.